

Contents lists available at ScienceDirect

Energy

journal homepage: www.elsevier.com/locate/energy



n-Butanol and Oleic Acid Methyl Ester, Combustion and NVH Characteristics In Reactivity Controlled Compression Ignition



Valentin Soloiu *, Aliyah R. Knowles , Cesar E. Carapia , Jose D. Moncada , Justin T. Wiley , Margaret Kilpatrick , Johnnie Williams , Mosfequr Rahman , Marcel Ilie

Department of Mechanical Engineering, Georgia Southern University, Statesboro, 30458, USA

ARTICLE INFO

Article history:
Received 25 February 2019
Received in revised form
27 May 2020
Accepted 18 June 2020
Available online 29 June 2020

ABSTRACT

Combustion, noise and vibrations produced by n-Butanol and Oleic Acid Methyl Ester (MO) in Reactivity Controlled Compression Ignition (RCCI) were investigated. The Cetane Number was determined using a Constant Volume Combustion Chamber (CVCC) for MO100, ULSD, and n-Butanol and found to be 73.8, 47.2, and 16 respectively. In the case of the MO20Bu80 (Methyl Oleate 20% with 80% n-butanol), the maximum Apparent Heat Release Rate was higher compared to ULSD Classical Diesel Combustion (CDC), due to accumulation of fuel in the combustion chamber because of the longer ignition delay and cylinder and charge cooling effect of n-butanol. RCCI with Methyl-Oleate had a vibrations level of as much 4.5 (m/s2) higher than ULSD in CDC up to 2k Hz. The sound level found by the Acoustic Array sound level for MO20Bu80 in combustion was 4 (dB) louder than ULSD in CDC. RCCI was found to have its own acoustic spectrum compared to CDC, and this is because of the wider range and higher sound levels produced by RCCI. The study suggests that MO can be used as a surrogate fuel for full body biodiesel in RCCI combustion.

© 2020 Elsevier Ltd. All rights reserved.

1. Introduction

Noise emitted from environmental, residential, and domestic sources, can be attributed, but not limited to aircraft, surface transportation, construction, rail, and manufacturing noise [1]. This occupational exposure is a leading cause of excessive noise levels that are generated by machinery and systems used in industrialized

Abbreviations: N, Piston normal force; F_{tr} Resultant force from masses in translation plus pressure force; β , Oscillation angle of connecting rod in relation to cylinder axis; K, Longitudinal force in Connecting Rod; F_{pr} , Pressure force on the piston; F_{itr} Total inertia force of parts in translation motion; T, Tangential Force at the crank pin; Z, Radial force in the crank pin; α , Angle of rotation of the crankshaft; β , Oscillation angle of the connecting rod measured from cylinder axis; ω , Angular velocity (radians); MO100, Neat Methyl Oleate; MO20Bu80, MO 20% by mass Butanol 80%; ULSD, Neat ULSDE in combustion; RCCI, Reactivity Controlled Compression Ignition; NVH, Noise Vibration Harshness; CPB, Constant Percentage Bandwidth; FFT, Fast Fourier Transform; dB (A), Decibel with A weighting; P, pressure; COV, Coefficient Of Variability; SMD, Sauter Mean Diameter; ID, Ignition Delay; CD, Combustion Delay; TDC, Top Dead Center; IVC, Intake Valve Close; EVC, Exhaust Valve Close; IVO, Intake Valve Open; EVO, Exhaust Valve Open; PFI, Port Fuel Injection; CVCC, Constant Volume Combustion Chamber; CDC, Classical Diesel Combustion; OSHA, Occupational Safety and Health Administration.

Corresponding author.

E-mail address: vsoloiu@georgiasouthern.edu (V. Soloiu).

societies. While few studies have been conducted to determine the magnitude of number of people being regularly exposed to occupational noise, hearing loss due to regular, systematic exposure has been documented since before the Industrial Revolution, circa the 1700 [1]. The U.S. Environmental Protection Agency (EPA), Federal Aviation Administration (FAA), and Federal Highway Administration (FHWA), along with other federal and local governmental agencies, have implemented environmental noise codes to lower day-night average sound levels (DNL) to adequately protect the public from excessive noise levels that can cause hearing loss due to prolonged exposure [1]. Occupational Safety and Health Administration (OSHA) provides guidelines for a safe work space and general environment. They mention that humans can hear a change in sound at around 3 dB (A) [2].

Diesel engine combustion noise can be attributed, but not limited to, load, speed, injection strategy, and fuel type to name a few. In this study, the dual injection strategy Reactivity Controlled Compression Ignition (RCCI) was used with alternative fuels. RCCI focuses on the use of a low reactivity fuel (such as an alcohol) to achieve near homogenous air and fuel in cylinder mixture, low temperature combustion with multiple ignition points, and controlled flame propagation by injecting the low reactivity fuel into the intake engine manifold, with direct injection of high-

reactivity fuel during the compression stroke [3,4]. These multiple injection events create a gradual heat release rate, low temperature heat release, and variable local ignition delay to eliminate non-homogeneous regions, ultimately reducing combustion temperatures. The renewable fuels used in this research were n-butanol, the low-reactivity fuel, and Methyl-Oleate (MO), used as the high reactivity fuel. Methyl-Oleate is a fatty acid methyl ester of the Oleic Acid and has been chosen as a surrogate for multi-fatty acids methyl ester (full body biodiesel) because of the Cetane number medium values easier control. The n-butanol is obtained from non-food sources and agricultural waste, and has desirable combustion characteristics such as low NOx and soot, making it a dependable, potential alternative and sustainable and renewable fuel candidate.

In previously conducted research [5,6], it was determined that various fuels and/or the injection strategy can produce differences in the engine noise and vibrations spectrum that can be recorded by specialized instrumentation: microphones, transducers and accelerometers. Soloiu et al. found that the fuel blends chemical properties will have a stronger influence than the mechanical components over the NVH characteristics of combustion events [6]. The type of fuel and blending, the reference methyl ester and nbutanol chosen, determined how the fuel's composition affected the vibrations and this was never studied by any research team. In addition, changing the two primary injection strategies allowed more accurate identification of specific sources and locations of noise & vibrations [7]. Preliminary to NVH analysis, in cylinder pressures, pressure gradient, and apparent heat release rates (AHRR) were investigated together with fuel characteristic analysis and fuel injection strategies to draw information for the NVH analysis and they are presented in the following chapters.

2. Literature review

2.1. Noise and vibration in engines review

Arnon et al., [8] stated that the vibration range between 500 and 1100 Hz had high correspondence values to the cylinder direction. This is because the variation in engine speed and load do not have an effect on this specific frequency range. Furthermore, the frequency range selected for their paper proved to be unaffected by the engine operating conditions. In addition, they found that the accelerometer placed in the vertical (cylinder) direction allowed for the vibration measurement of the combustion process. By using a geometric model, Kim and Lee [9] noticed that the most noticeable noise came from the compression wave after the intake valve closing. This was found by using a simulation to model the pressure waves produced in the cylinder after the compression stroke. They used a Lagrange interpolation method to allow for better ease of mesh refinement. Badwi et al. [10] found that the inlet and exhaust valves close with the same vibrations frequency at 3500 Hz and open at 1400 Hz with a simulation of a single cylinder diesel engine at 700 RPM over the course of multiple cycles across time. They also stated that the gas dynamics contributes to the engine vibration. Miura et al. [11] found that a four-cylinder in line diesel engine operating at idling conditions, has noise characteristics that are heavily influenced from piston slap and the mechanical noise more so than from combustion. The valve train also was the most major noise source. The gear rattling is due to the camshaft drive torque. Goldwine et al. [12] states that the peak vibration potentially measurable on a variety of an engine envelope performance. Goldwine et al.'s paper concludes that the ignition timing is an important factor to study.

Wissink et al. [13] says the ringing noise created by CI (compression ignition) strategies primarily originates from circumferential pressure waves. The overall lower noise and power

spectral density of RCCI (reactivity controlled combustion ignition) is due to the increased reactivity stratification. This increases the changes in ignition delay, and it elongates the heat release event and the peak of the heat release rate lowers. The in cylinder combustion pressure, the IVC, the EVC are the most noticeable excitation sources on the cylinder head [14,15]. The valve train noise was found to be produced by the gear noise rattling. This also agrees with Miura et al. [11] when it comes to the changes in the camshaft drive torque. A paper by Chen [16], states that at lower speeds, the largest noise can come from the valve train noise, and the valve train noise can correlate to the natural frequencies of the valve system. He also notes that the impact of the piston to the cylinder is the largest noise source from a mechanical point-of-view. The piston slap depends the most on the maximum pressure in the cylinder and the tolerances between the cylinder and the piston. He also adds that the in cold start and idle conditions the slap noise is the most prominent if the cylinder to piston gap is relatively large. In the table below, he also gives the main frequency ranges of noise sources for automotive engines.

Adams [17] calculated that an accelerometer, or any displacement transducer, applied to a surface that has rotating component attached would produce a periodic signal based on the rotational action of the attached piece. In a study by Soloiu and Jenzer [18] showed that the active control of torsional vibration is possible through the pilot injection and delayed combustion timing, and this has brought about the possibility of using delayed injection timing in the combustion process in order to control the vibrational harmonics. The authors are paving the way for the possible considerations of using the various novel injection strategies and timings to adjust the vibrations and sound produced. In a paper by Kimura et al. [19], the study produced results that attributed impact noise and vibration to the influence of the crankshaft on the thrust bearing made by the axial and torsional vibration of the crankshaft. This occurred at the 4.5th, 6th, and 9th orders in their chosen test bed. Their conclusion is that the torsional vibration is a primary cause to the axial vibration.

In a research conducted by Soloiu et al. [7], with RCCI and NVH study, he used S-8 synthetic kerosene as high reactivity fuel and nbutanol as the low reactivity fuel. Their baseline fuel was ULSD#2 in RCCI with n-butanol. They found that the results from the crank angle analysis depend on fuels' properties in the lower frequency range for combustion. In the overall experiment, the authors found that the synthetic kerosene was a viable fuel based upon the overall sound produced by both fuels. In that paper, the multi-field microphone was placed in the direction perpendicular to the single cylinder axis. In another research paper by Soloiu et al. [5], the piston normal curve was determined and the piston slap in the cylinder correlated with the sound levels produced in the cylinder axis. A paper by Dolatabadi et al. [20] supports these results. In a paper by Shahabuddin et al. [21], they used biodiesel to show the effects of its properties on engine performance. Howarth et al. [22] states that having both vibrations and noise measurements are beneficial to have a more accurate "prediction" of the total disturbance in a NVH evaluation. The study suggests to keep NVH measurements less than a few minutes at lower vibration levels. They showed that the biodiesel and its blends have an effect on the heat release rate and peak cylinder pressure are due to the lower heating value of the biodiesel, this was based on its shorter ignition delay biodiesels have lower compressibility, higher viscosity, and cetane number.

2.2. Beamforming literature review

The technique used in this paper is Beamforming or Statistically Optimized Near-field Acoustical Holography (SONAH). SONAH

benefits its user by being able to perform in low-frequency ranges and maintain a low sensitivity to sources outside the calculation plane with non-uniform grid of microphones [23]. Beam forming is beneficial because the basis is on the arrangement of microphones. One of the ways a wider frequency range can be achieved is by arranging the microphones in a simulated random positions that uses identical segments that are randomly optimized for the best results [24,25].

In addition to the knowledge of source location, the microphone locations used for the array were chosen because the frequency range is the human hearing range. The "average beamforming approach" was used because the equipment for this particular research is for indoor or in-cabin situations [26]. In terms of signal processing data from multiple signals, beamforming allows specific weights to within this study to determine the spatial filtering characteristics. Much like the Acoustic Array, the beamforming process filters some of the frequency signals that overlap and originate from different locations. To provide the statistically optimum results with these weights, it is best to provide adaptive algorithms that will accomplish finding the weights appropriate for the source and signal amount. However if there is a large amount of sensors to consider, then computational considerations must be made in the form of partially adaptive beamforming [27]. For the FFT in beamforming, it has to be using a set of beams (or signals) that are fixed, non-overlapping, and simultaneous. If a "spatial FFT," is used the case would mean that FFT beamforming is in terms of space rather than the frequency in which the signals occur [28].

3. Fuel properties

3.1. Physical and chemical properties

The fueling research of the engine with the common rail RCCI injection strategy consisted of port fuel injection of n-butanol 80% by mass and 20% by mass of Methyl Oleate (MO20Bu80). As a reference fueling condition, ULSD#2 was in Classical Diesel Combustion (CDC) mode. In table two, a summary of the fuel properties is provided and the following subsections will discuss some of the

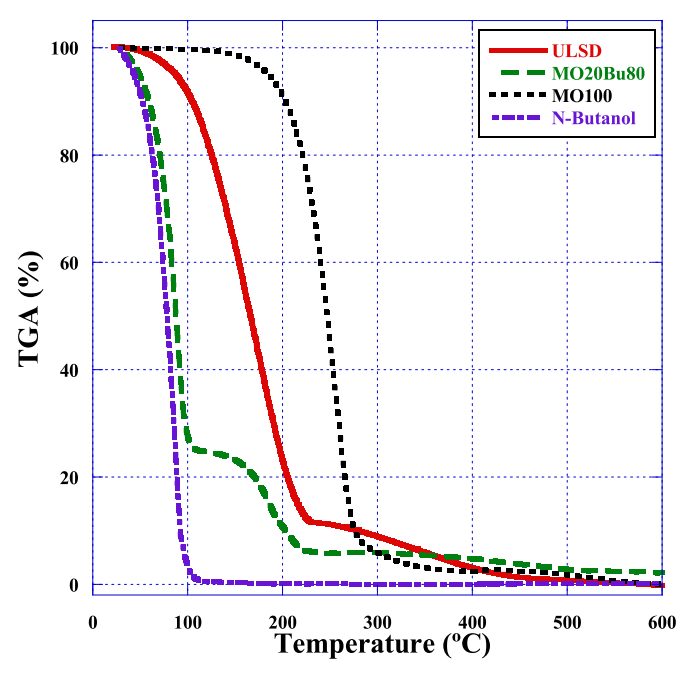


Fig. 2. Thermal gravimetric analysis.

data acquired for this table.

The fuels cetane numbers were determined in house using a PAC CID 510, Constant Volume Combustion Chamber (CVCC) [29,30]. The American Society for Testing and Materials (ASTM) [31] standard recommends the following equation (1) to calculate the cetane number obtained by experimentation. This standard requires the use of a constant volume combustion chamber. The equation determines the DCN (derived cetane number) by converting the ignition delay (ID) average and combustion delay (CD) average after 15 cycles by using the multivariable equation seen in equation (1).

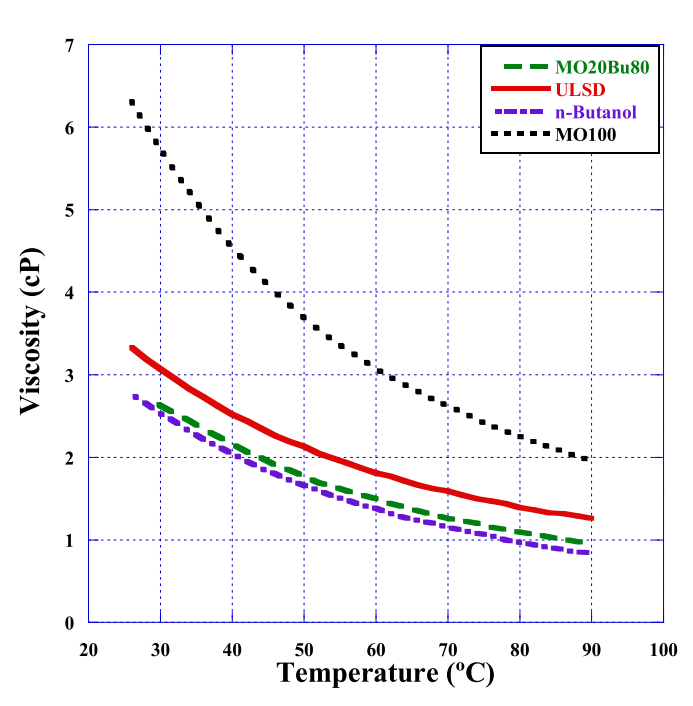


Fig. 1. Viscosity vs Temperature.

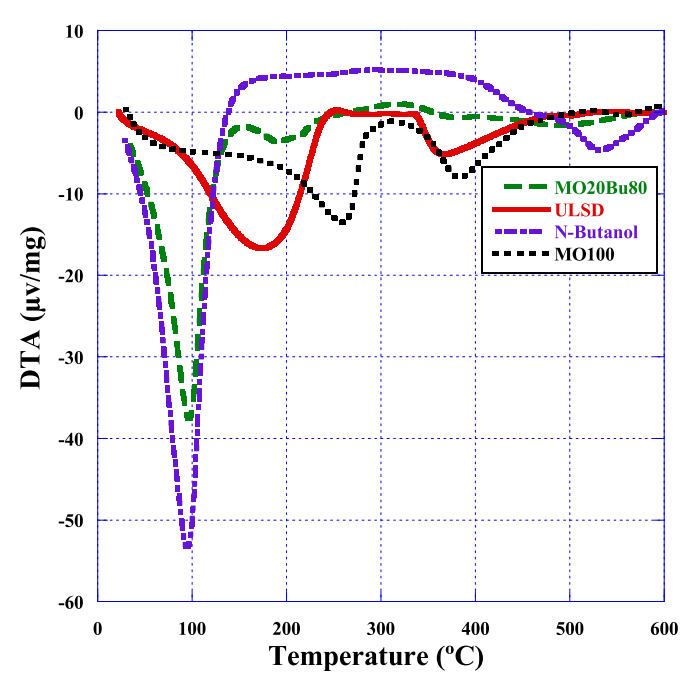


Fig. 3. Differential thermal analysis.

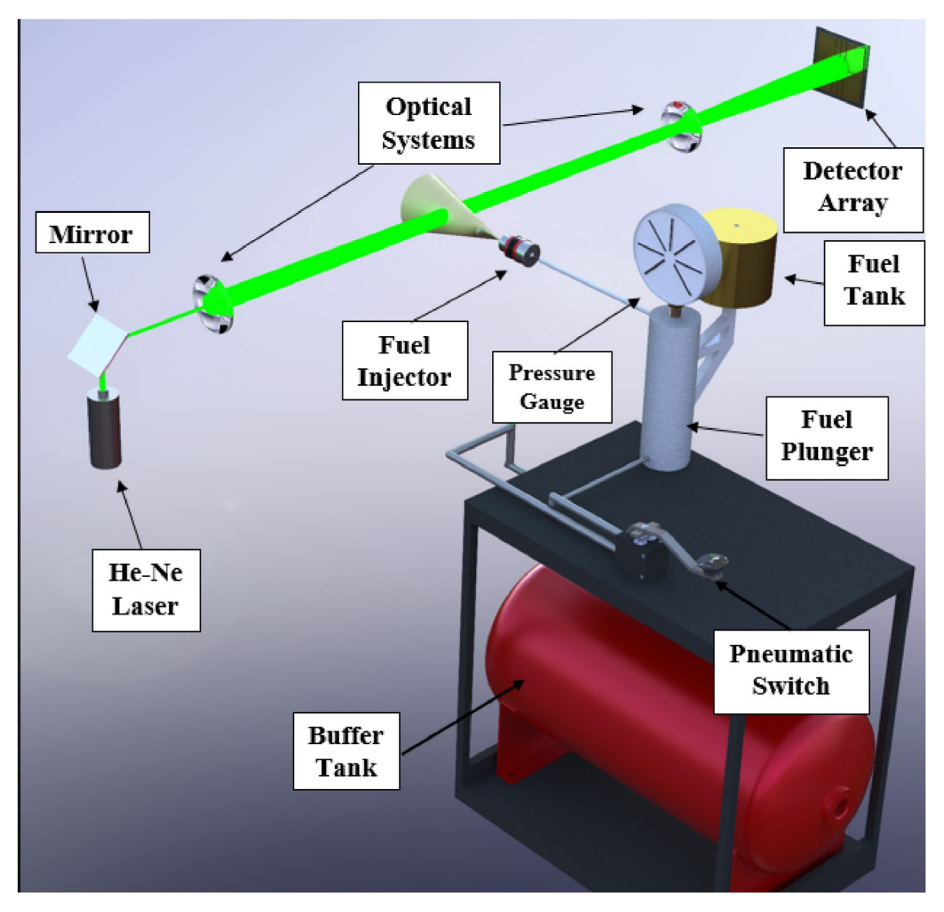


Fig. 4. Mie scattering He—Ne laser, experimental set-up.

$$\begin{split} \textit{DCN} &= 13.028 + \left(\frac{-5.3378}{\textit{ID}}\right) + \left(\frac{300.18}{\textit{CD}}\right) + \left(\frac{-1267.90}{\textit{CD}^2}\right) \\ &+ \left(\frac{3415.32}{\textit{CD}^3}\right) \end{split} \tag{1}$$

According to a paper by Knothe et al. [32], they determined that the fatty ester compounds derived from branched alcohols have improved low temperature properties over the straight-chain alcohols. The authors also found that the methyl oleic acid had a cetane number of 59.3 based on one of their preferred standard of ASTM D613. In a paper by Han et al. [33], diesel to has the lowest density and viscosity when compared to methyl Oleate and Laurate. The authors wrote that the differences in injection delay found among their test fuels was because of the viscosity, fuel density, and bulk modulus of compressibility. The pressure oscillation damps more rapidly for Methyl Oleate due to the aforementioned properties. The DCN numbers for MO100, ULSD, and n-Butanol were 73.8, 47.2, and 16 respectively.

As can be seen in Fig. 1, MO 100 has the highest viscosity among the other fuels tested. This is significant because the viscosity will have an effect on the atomization during the injection and ignition delay. A study conducted by Jiaqiang et al. [34], showed that the kinetic viscosity can have an effect on ignition delay and the relationship saturation levels and combustion as well. The viscosity of the MO20Bu80 is slightly higher than n-butanol, however the values of viscosity of MO20BU80 more closely resemble that of ULSD than MO100. The tests were over a range of temperature between 22 °C and 90 °C.

Thermal Gravimetric Analysis (TGA) (shown in Fig. 2) and Differential Thermal Analysis (DTA), (shown in Fig. 3) were tests used

to evaluate the vaporization characteristics and the endothermic and exothermic reactions of the fuels respectively. The tests were over a range of temperature between 23 °C and 600 °C. The TGA-DTA tests were with a Shimadzu DTG-60 (error $\pm 1\%$, accuracy ± 1). The vaporization curve (TGA) shows that n-butanol vaporizes

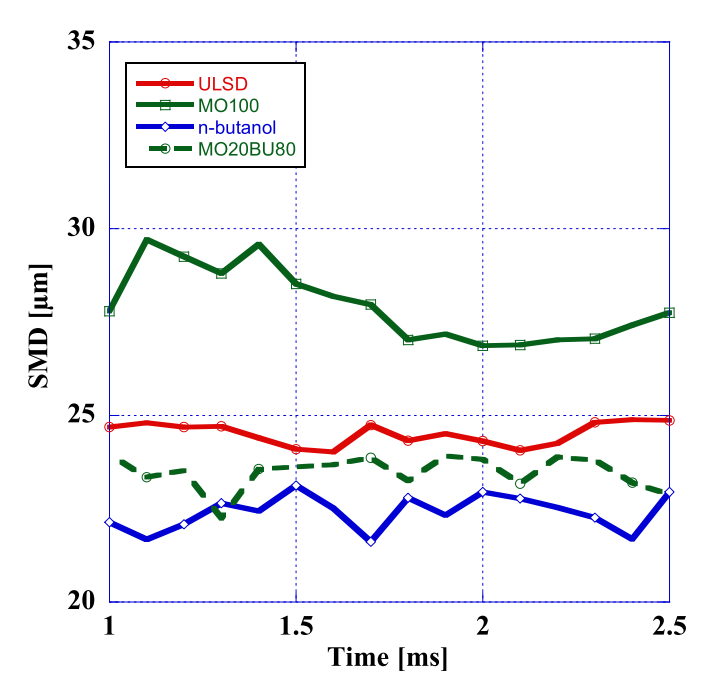


Fig. 5. Sauter Mean Diameter vs Time.

Table 1Typical frequency range of primary noise sources of automotive engines [16].

Noise Source	Frequency (Hz)	Observations
Combustion Noise	500-8000	Depends on engine load
Piston Slap Noise	2000-8000	Depends on speed and # of cycle
Intake/exhaust Valve	500-2000	Depends on speed and valve design
Cooling fan	200-2000	Depends on blades speed and # of blades
Intake	50-5000	Periodic intake>200 Hz > intake turbulence < l kHz
Exhaust	50-5000	Exhaust turbulence> 1 kHz
Injection Pump	2000	Depends on speed and pump
Gear	4000	Depends on speed and # of teeth
Accessory Belt	3000	Depends on speed, misalignment, slippage/friction coefficient
Timing Belt	3000	Depends on speed and # of teeth

quickly as the temperature increases, and MO20Bu80, due to amount of n-butanol (80% by mass of n-butanol), initially has a similar burn off as the n-butanol up to 130 °C. This burn off could be due to the effect of MO, as can be seen by the curve produced by MO100. This makes vaporization completion earlier for the MO20Bu80 [7,36,37].

In terms of the DTA, the data points that fall noticeably below zero correlate to endothermic reactions and the peaks correlate to the exothermic reactions. The fuel that has 80% n-butanol will have similar vaporization curve as pure n-butanol at (or close to) the 95 °C. The two-stage energy release for MO100 and ULSD originate from a lean mixture oxidation, and a decomposition of these fuels in the vaporization process. The heated environment induced by the temperature range causes this slow oxidation process. In this case, ULSD has a lower heat of vaporization than MO100; this is with the consideration that n-butanol, and the mixtures there of, will have the highest heat of vaporization at the lowest temperatures.

3.2. Mie scattering by He-Ne laser of spray and mixture formation

The spray has been analyzed by Sauter Mean Diameter (SMD), standard statistical analysis that evaluates the droplet size distribution and mean diameter of the droplets as the cloud moves away from the nozzle [38]. Atomization studies commonly use SMD to get a better understanding of the fuel's spray pattern and mixture development and was done on the neat versions of ULSD#2, Methyl Oleate and n-butanol along with a fuel mixture composed of 20% by mass of Methyl-oleate and 80% n-butanol. A Mie scattering He-Ne Laser was the primary equipment used for measuring the SMD history of the selected fuels coupled with a single injector nozzle at an injection pressure of 180 bar, utilized to provide a standardized SMD measurement process [7,37,39]. The fuel was injected into a standard atmospheric environment (1 atm) at room temperature (20 °C), and done so at least 15 times per fuel for data collection. The He-Ne Laser was used in conjunction with a collimating lens and a collector lens system to focus and collect the beam on to a 32 detector array. The data collection was done with a Malvern instrument at a sampling rate of 10 kHz. The size of the droplets were measured in micrometers (µm), utilizing a statistical analysis of data post processed with the Fraunhofer Diffraction Theory.

Table 2 Fuel Properties [31,35].

Properties	MO100	MO20Bu80	ULSD	n-Butanol (100%)
CN	73.8		47.2	16
Density g/cm ³	0.87		0.85	0.807
Ignition Delay	2.35 ms	0.86 ms	1.08 ms	
Viscosity @ 40 ℃	4.54 cP	2.16 cP	2.52 cP	2.04 cP
LHV (MJ/kg)	37		44.3	32.5

Table 3 Engine specifications, (axis origin: 0 deg, TDC in combustion).

Bore	112 mm
Stroke	115 mm
Number of Cylinder(s)	1
Compression Ratio	16:1
Max Power	23 HP @ 2200 RPM
Cooling System	Water
Number of Valves	2
Displacement	1.132 L
Exhaust Valve Open (EVO)	135 CAD
Intake Valve Open (IVO)	360 CAD
Overlap	360-375 CAD
Exhaust Valve Close (EVC)	375 CAD
Intake Valve Close (IVC)	585 CAD

The time in which data collection occurred was set at 1 ms after the initiation of the injection event and ended at 2.5 ms. A 3D schematic of the experimental set-up used is presented in Fig. 4. As seen in Fig. 5, the SMD for MO100 is on average 5 μm larger than ULSD which means that the droplets of MO100 have a smaller surface area than ULSD for the same mass of injected which would have an effect on ignition delay. This phenomenon was observed in the previous CVCC fuel analysis of the selected fuels where MO100 experienced an ignition delay of 2.35 ms versus ULSD at 1.08 ms. N-butanol was observed to exhibit a smaller SMD than that of MO100 similar to that of ULSD with the majority of the injection event occurring at a lower SMD.



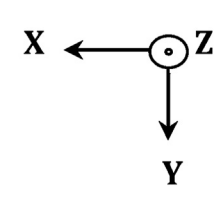


Fig. 6. Accelerometer placement on valve cover [5].

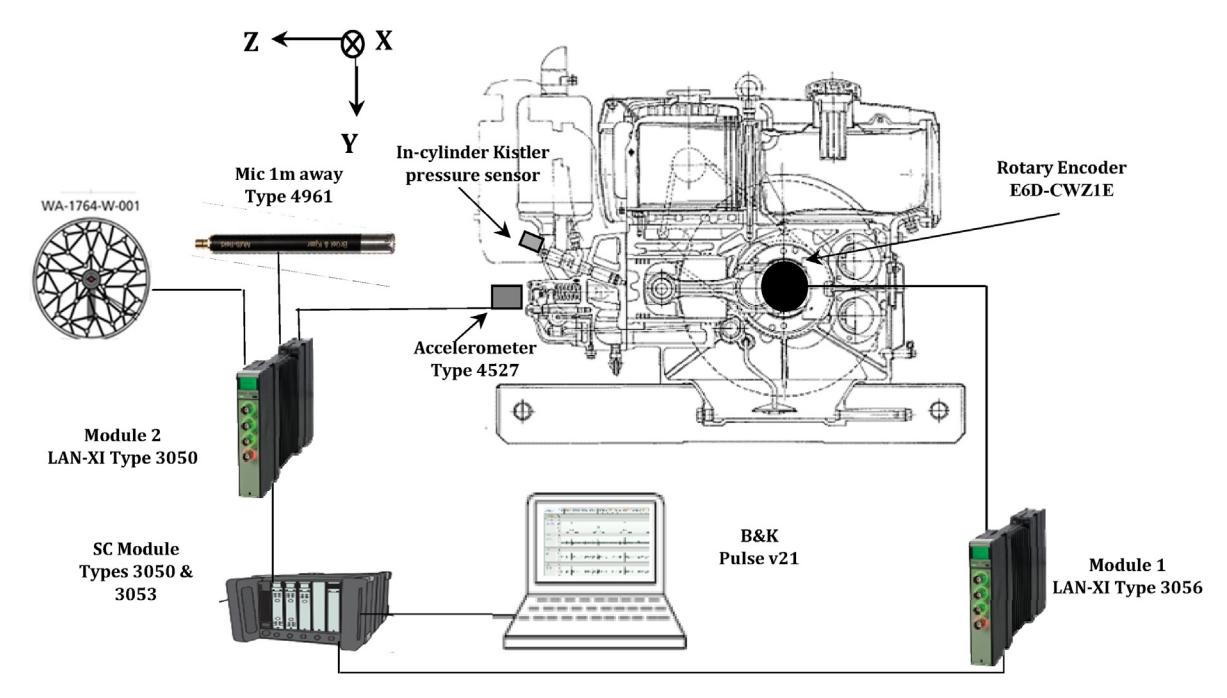


Fig. 7. NVH set up [5,6].

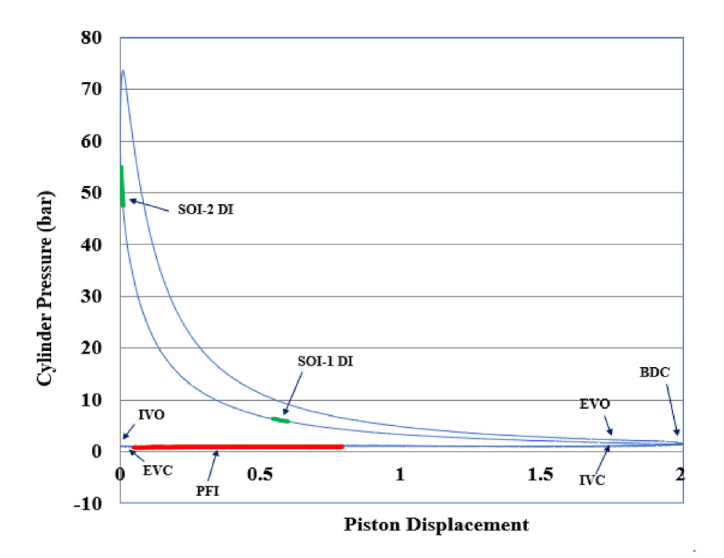


Fig. 8. P-V diagram with injection timing and durations in RCCI.

4. Experimental methods

4.1. Experimental engine set-up and NVH set-up

The research in this paper used a single cylinder DI

experimental engine instrumented with a common rail system [29,39], a Kistler 6053 cc piezoelectric uncooled pressure sensor with a Kistler Type 5010 signal amplifier, an OMRON 3600 pulse rotary encoder, and Bruel & Kjaer (B&K) transducers (see Table 1). The B&K transducers involve: an acoustic array (Type 9712 W FEN) with thirty array microphones (Type 4959), one condenser type multi-field microphones (Type 4961), and a tri-axial accelerometer (Type 4527). The data acquisition systems used for the array were B&K Types 3660-C-100, 2831, 3050-A-060-X, 3053-B-120-X, UA-2112-060, and UA-2112-120. The data acquisition systems used for the accelerometer and multi-field microphone analysis were B&K Types 3050 and 3056. The primary software used to study the NVH levels produced by the research engine was PULSE Reflex v21. Combustion analysis was done with an AVL INDICOM and a YOKOGAWA DL850 DAQ system for the Kistler sensors and Omron sensor. The sensors have been chosen to cover the frequency spectrum presented in Table 1 using fuels with characteristics presented in Table 2. To view the experimental engine specifications, see Table 3

The accelerometer was placed on the valve cover of the engine as seen in Fig. 6. With the Z-axis is parallel to the piston axial motion direction (parallel to cylinder axis), and the X-axis is going through the center of crankshaft axis and parallel to it. The Y-axis was the vertical perpendicular on the crankshaft and cylinder axis. The multi-field microphone was parallel to Z direction and perpendicular to the X-Y plane. The microphone was set at 1000 mm placement away from the engine. The placement of the

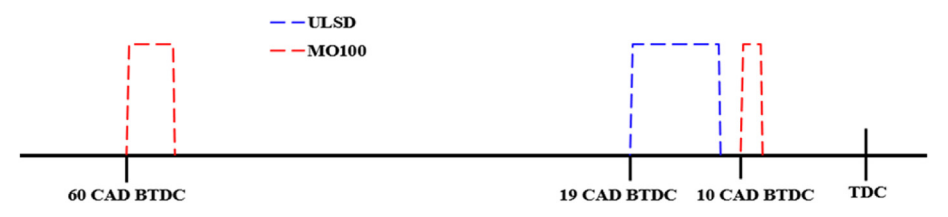


Fig. 9. Direct injection scheme for RCCI and CDC for all fuels (rate of injection vs CAD).

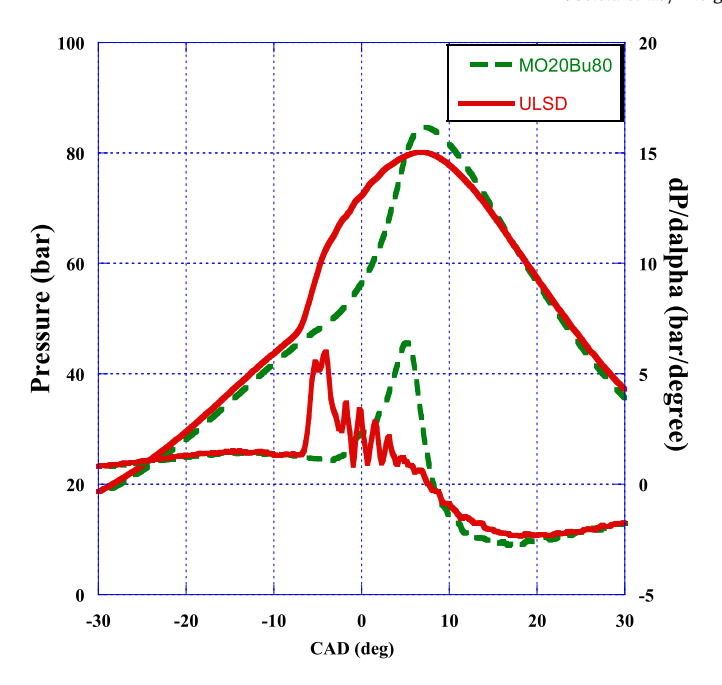


Fig. 10. In-cylinder pressure and pressure gradient vs crank angle.

acoustic array was identical to the to the multi-field microphone placement (see Fig. 7).

4.2. NVH analysis

Constant Percentage Bandwidth (CPB) and Fast Fourier Transform (FFT) analysis were at the forefront of the sound and vibration analysis. For the crank-angle-domain analysis the pressure, rotary encoder and the microphones were used to obtain data. In the crank angle domain, analysis the combustion was set to 0° TDC reference. Array analysis, much like the CPB, brought more detail in to the data analysis by looking at each frequency within the

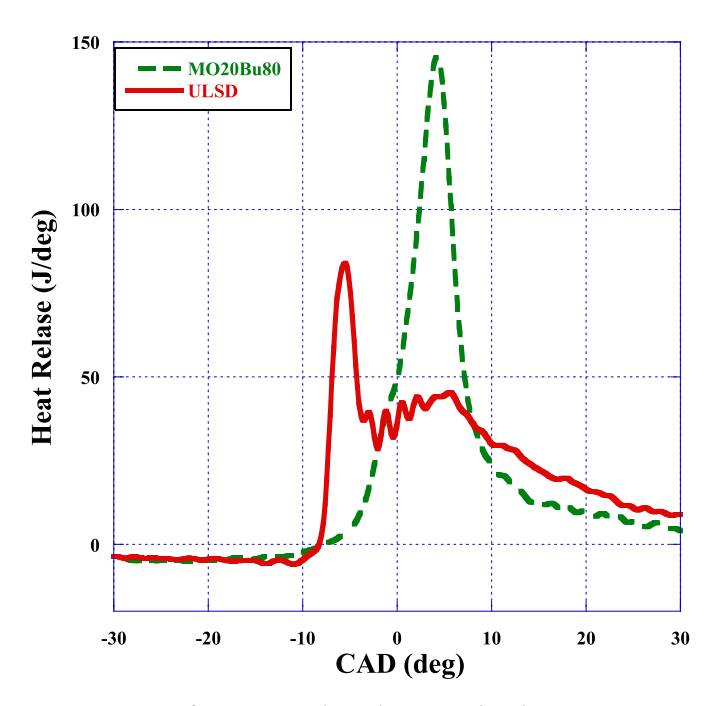


Fig. 11. Apparent heat release vs crank angle.

combustion range of 250 Hz to 2.5 kHz. By looking at the overall sound emitted by the engine, a better comparative analysis of the fuels was obtained, and the overall study of the sound produced by the engine used beamforming and a delay and sum calculation within the B&K Pulse v21 program. The accelerometer data had a crank angle analysis and FFT analysis. The reference point (zero is TDC) was the same as the microphone reference point [40].

4.3. Procedure

The NVH measurements were made at 1500 RPM at 6 bar indicated mean effective pressure (IMEP) for 15-s increments. The Coefficient of Variability (COV) for RCCI with Methyl Oleate was 2.06. The COV for ULSD with classical combustion was 1.14. The recording frequency span was at 25.6 kHz for the crank angle analysis and 25.6 kHz for the acoustic array analysis.

4.4. Fuel injection strategies

In Fig. 8, the P-V diagram provides a description of the injection timings during the cycle. PFI of n-butanol was delivered at 340 CAD

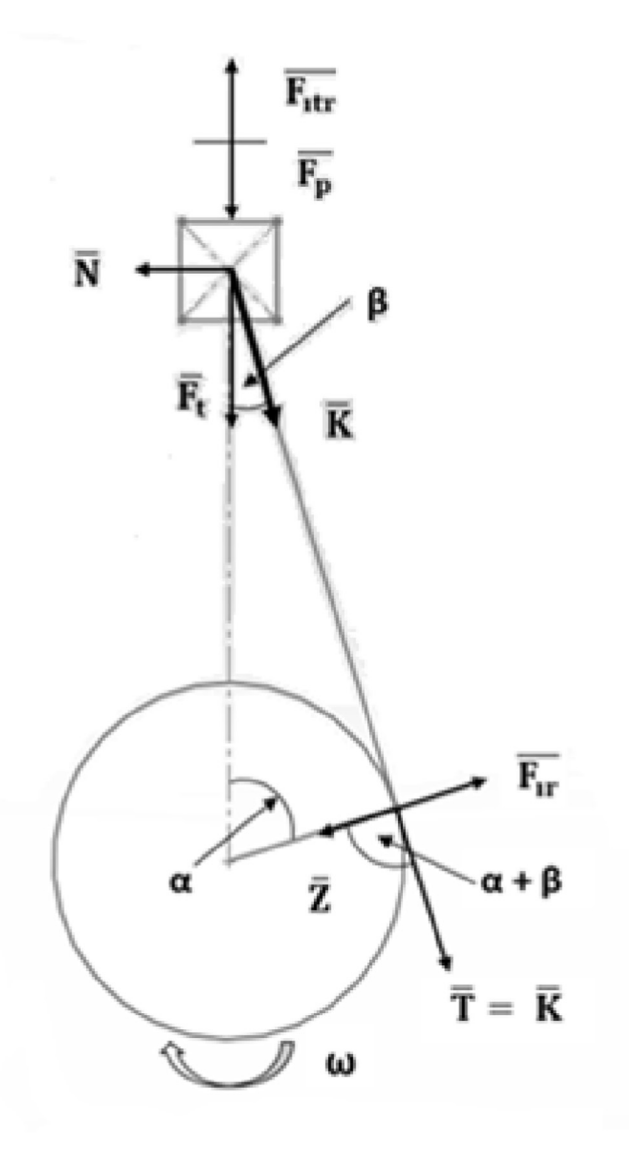


Fig. 12. Engine dynamics.

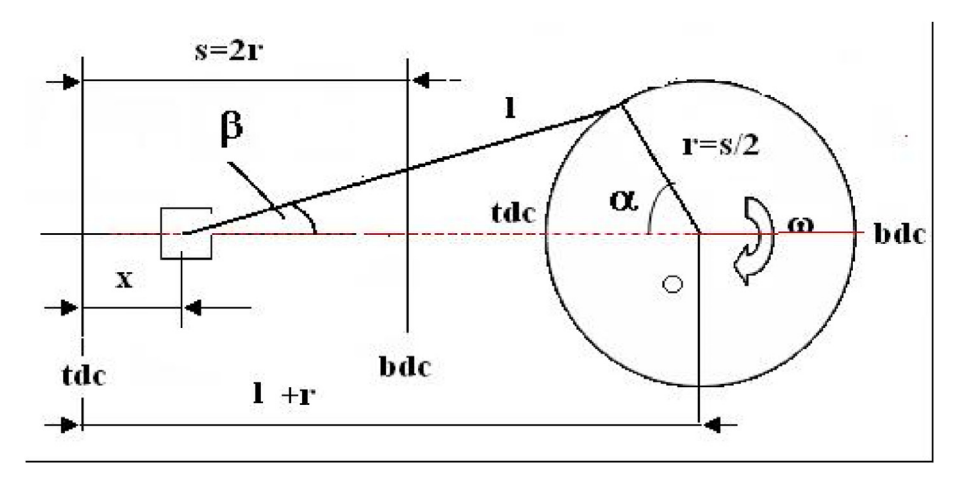


Fig. 13. Engine kinematics.

BTDC, which is 5 CAD after exhaust valve closing. For a range of 345 to 300 CAD BTDC, the PFI timing was chosen to improve combustion stability, reduce exhaust scavenging, and increasing the timing led to a rise in COV of IMEP and unburned hydrocarbons. The mass of n-butanol PFI for RCCI was determined to be 80% by mass for Methyl-oleate to maintain a CA50 of 6° ATDC. COV beneath 5%, and the optimization of pressure gradient dp/dalpha. The optimization of dp/dalpha with PFI% was studied by Liu et al. where it was found that a higher PFI % led to a decrease in dp/dalpha due to a shift in combustion phasing of RCCI [41]. The effect PFI% has on combustion is not only related to pressure but also on emissions as well, and was investigated by Zheng et al. where it was found that a higher percentage of n-butanol led to the reduction of emissions of soot [42]. This ratio for (MO20BU80) was carefully selected based off the high reactivity of Methyl-oleate and low reactivity of n-butanol that was observed from both the Constant Volume Combustion Chamber analysis and the following literature sources [30,43–45]. The DI two injections, shown in green, are for controlling the emissions in RCCI mode as well as reducing dp/dalpha. The reduction of dp/ dalpha with an optimized DI strategy for RCCI was observed by Liu et al. where a reduction of mass injected per injection event led to a decrease in dp/dalpha from the decrease in knocking events [46]. In Fig. 9, ULSD has a singular injection event only, that is set at the engine's OEM specifications in order to maintain the CA50 timing while for MO100, the first injection pulse was utilized along with the secondary injection to help facilitate RCCI together with the nbutanol PFI during the intake stroke as previously stated at 80% by mass of the total fuel injected.

The duration for the first injection event was optimized taking into account some results by Han at al [47]; where it was shown

that Methyl-oleate mass injection rate closely resembled ULSD's mass injection rate given a moderate injection pulse-width. However, the second injection event's duration is directly controlled by the ECU's speed controller in order to maintain a steady 1500 RPM with only minor differences in injection duration per cycle. The slight difference in injection duration corresponds to the findings by Han at al. [48], where it is shown that the time in-between SOl-1 and SOl-2 injection events has an influence on the mass injected from the effect of the common rail pressure waves caused by the pilot injection.

5. Results and discussions

5.1. Combustion results

The results presented for the combustion analysis are those with most influence on the engine NVH: in-cylinder pressure and pressure derivative as seen in Fig. 10, the heat release, and NVH comparisons. ULSD results are represented in red and MO20Bu80 in green throughout the paper. In Fig. 10, the Pressure derivative are the bottom lines and the top two lines are the in-cylinder pressure [30].

The in-cylinder pressure graphs show that the RCCI injection strategy has a higher pressure rise than ULSD. This happens due to the delayed combustion by the n-butanol that absorbs a high amount of heat for vaporization and has a very low cetane number. In the initial pressure rise rate the ULSD in combustion showed a higher-pressure rise rate per CAD than MO20Bu80 [30]. In Fig. 11, the heat release graphs are presented. In terms of the MO20Bu80 heat release, because of, the longer ignition delay from n-butanol

Table 4 Equation list for engine dynamics.

Equation	Name	Number
$\mathbf{x}_{\mathbf{p}} = \mathbf{r} \left[(1 - \cos \alpha) + \frac{\Lambda}{4} (1 - \cos 2\alpha) \right] [\mathbf{m}]$	(Piston position)	2
$W_p = \mathbf{r} \cdot \omega \Big[\sin \alpha + \frac{\Lambda}{2} \sin 2\alpha \Big] \qquad [\mathbf{m}/\mathbf{s}]$	(Piston Velocity)	3
$a_{grp} = r \cdot \omega^2 (\cos \alpha + \Lambda \cos 2\alpha) [m/s^2]$	(Group piston acceleration)	4
$F_{p}(\alpha) = \frac{\pi}{4} \cdot D^{2}[p(\alpha) - p_{crankcase}]$ [N]	(Force on Piston)	5
$F_{itr} = -m_{tr}a_{grp} [N]$	(Inertia Force of piston group)	6
$F_t = F_{itr} + F_p [N]$	(Total Force on the piston)	7
$N = F_t \cdot \tan \beta$ [N]	(Piston Normal Force)	8
$K = \frac{F_t}{\cos\beta} \qquad [N]$	(Longitudinal Force in the Connecting Rod)	9

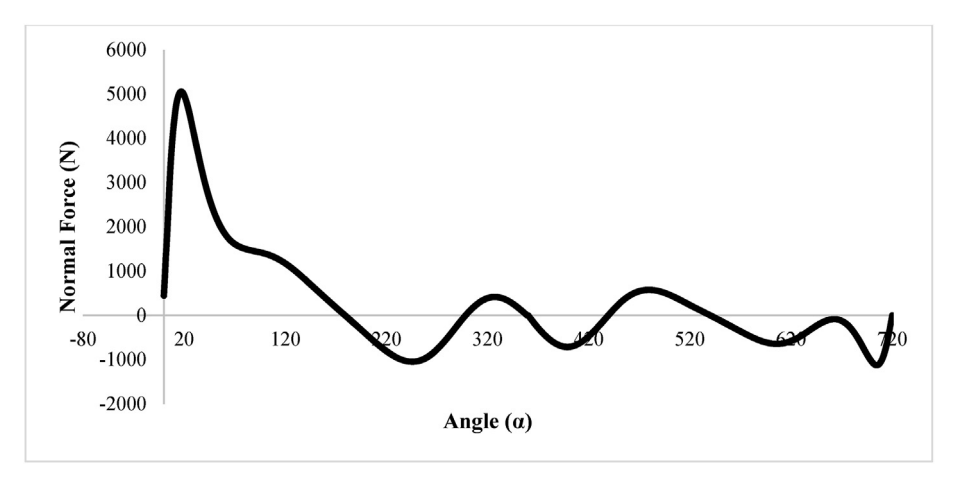


Fig. 14. Piston normal force on the cylinder wall/skirt.

(due to cooling effect of n-butanol seen also in compression pressure BTDC in Fig. 10), and the higher reactivity of Methyl-Oleate as observed from the CVCC's investigation, and the effect of oxygen content on Methyl-Oleates reactivity from a lowered ID as observed by Allen at al. [45], the maximum apparent heat release rate (AHRR) is much higher due to accumulation of fuel in the combustion chamber and Methyl-Oleate's high rate of combustion, as seen in Fig. 11 [30]. In conjunction with the diffusion stage of combustion, while it is very visible with ULSD, in the case of MO20Bu80 it disappears showing only a very large premixed phase of burn.

5.2. Theoretical application

Identifying the origins of the sound produced by the engine during combustion was required and a theoretical study of the piston normal force and a breakdown of the forces are presented in the Figs. 12 and 13, and Equations in Table 4. By deriving the reciprocating motion, the piston acceleration has been obtained. Once the forces were acquired, the piston normal force variation was used for correlation with the combustion sound analysis. The piston's normal force (on the skirt) found in this study is presented in Fig. 14. In addition, the piston does not land flush to the cylinder when it progresses in translation through the cylinder; the piston undergoes a tilt that forces the top and bottom edges to hit the sides of the cylinder. See Fig. 15 for more details. The equations used to obtain the piston normal force on the cylinder are equations 2-9 in Table 4. In addition, Fig. 16 has the exhaust valve and intake-valve-lift profile [49].

5.3. Campbell plot analysis

For the NVH study, all comparisons for the vibrations correlates with the Piston Normal Force Curve shown in Fig. 14 and with the Valves' Timing, shown in Fig. 16. These two processes are key to allow some mechanical correlations to be determined during the engine cycle. In Fig. 15, the piston tilt has been amplified for better understanding of the slap produced. During this tilt, the top of the piston and the bottom of the opposite edge of the skirt slap the cylinder and produce vibrations. The recorded noise from the slap of the piston skirt has been presented in Fig. 17 at 90 CAD and 450 CAD where individual colored circles represent an engine cycle.

For the noise side of the NVH study, the sounds produced during the cycle are presented in Campbell plots that show that there are

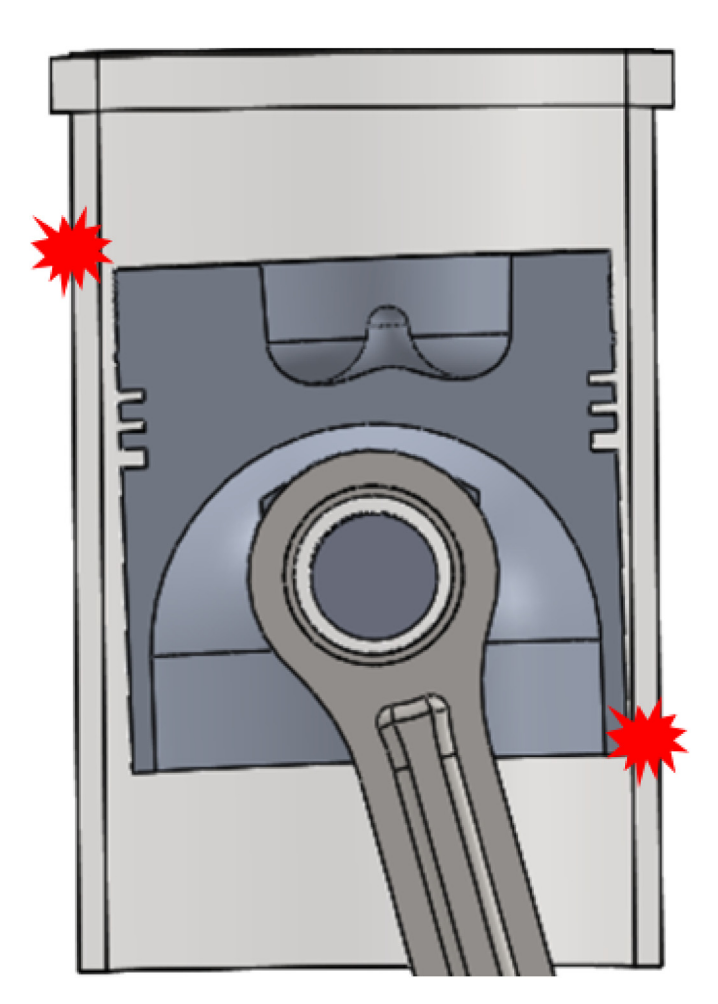


Fig. 15. Piston slap during crank progression.

differences produced by the combustion characteristics of each fuel. The graphs from Figs. 17–19 can be interpreted as follows: the X-axis of the graph is following the crank angle during the engine's cycle, with 0 as TDC in compression, the left vertical Y-axis represents the cycle number during recording, and the right hand side Y-axis represents the intensity level of the data (acceleration or sound pressure) measured by the equipment. To further assist in

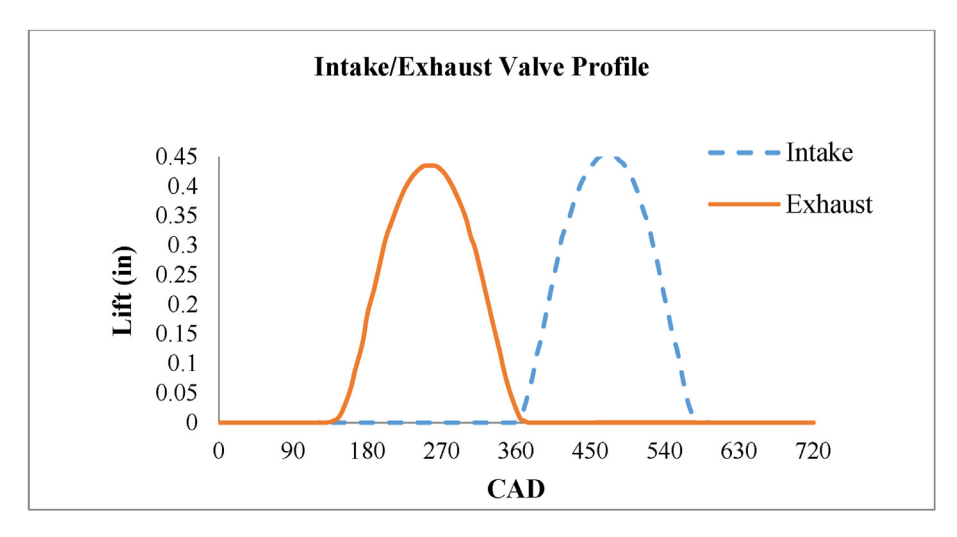


Fig. 16. Valve lift vs crank angle.

understanding the data representation in the Figs. 17–19: the diameter of the circles depends on the duration of the sound (in crank angle degrees) and each circle is produced in a different cycle. Initial legend concerning various sound sources in the engine is given on X axis of Fig. 17.

In Fig. 17 the bands for sound during the cycle are presented. At 10 CAD after 0 (TDC) the combustion noise is recorded in the first band. The next vertical band has the piston slap which occurs at the 90 CAD mark. Slightly before 180 is the sound from the EVO opening, and the 360 CAD is the IVO and start of valve overlap, which ends at 375 CAD. At 450 CAD is the next noticeable piston slap (force on the skirt). At 540 CAD the intake valve closes, and at

10° before 720 CAD the injection event occurs [50].

When one looks closely at the sound levels produced by the engine with each of these fuels, there is a significant difference between ULSD and MO20Bu80 in combustion (Fig. 18). In the cylinder direction (Z-axis), MO20Bu80 in combustion the sound is the highest with pressure measurements as high as 10 Pa. USLD in CDC has a sound level much lower at 3.2 Pa. This is due to the RCCI producing more noise in the cylinder due to the physical and chemical properties of the fuels and the RCCI combustion characteristics. The higher heat release rate for MO20Bu80 that is almost double of that of the ULSD and the pressures waves from MO20Bu80 propagating in the cylinder during combustion.

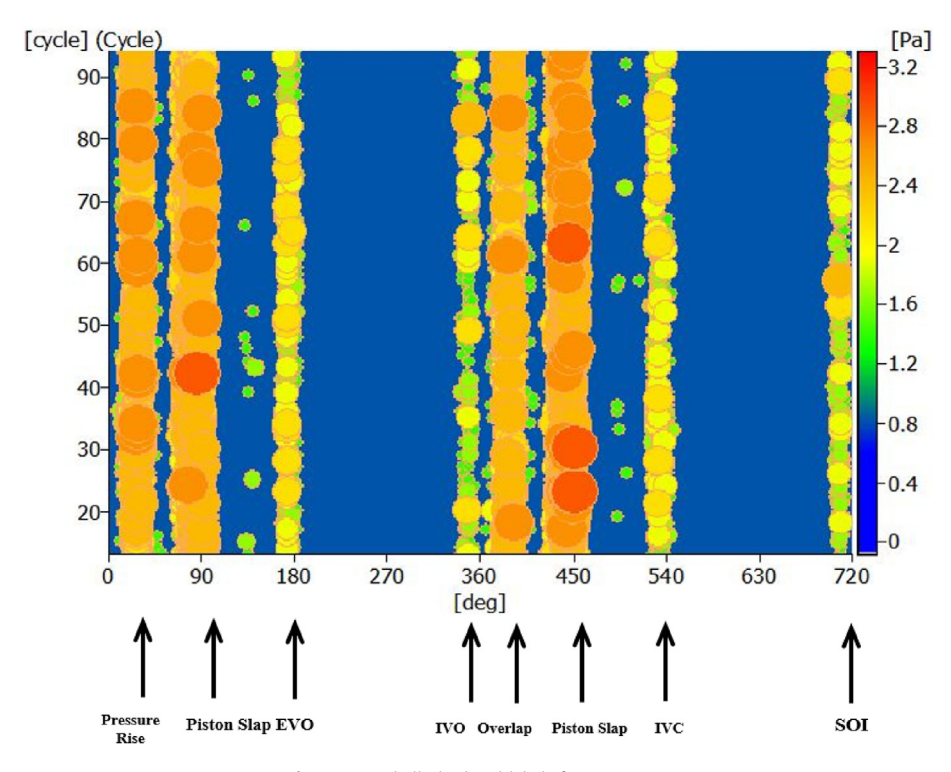


Fig. 17. Campbell plot band labels for ULSD CDC.

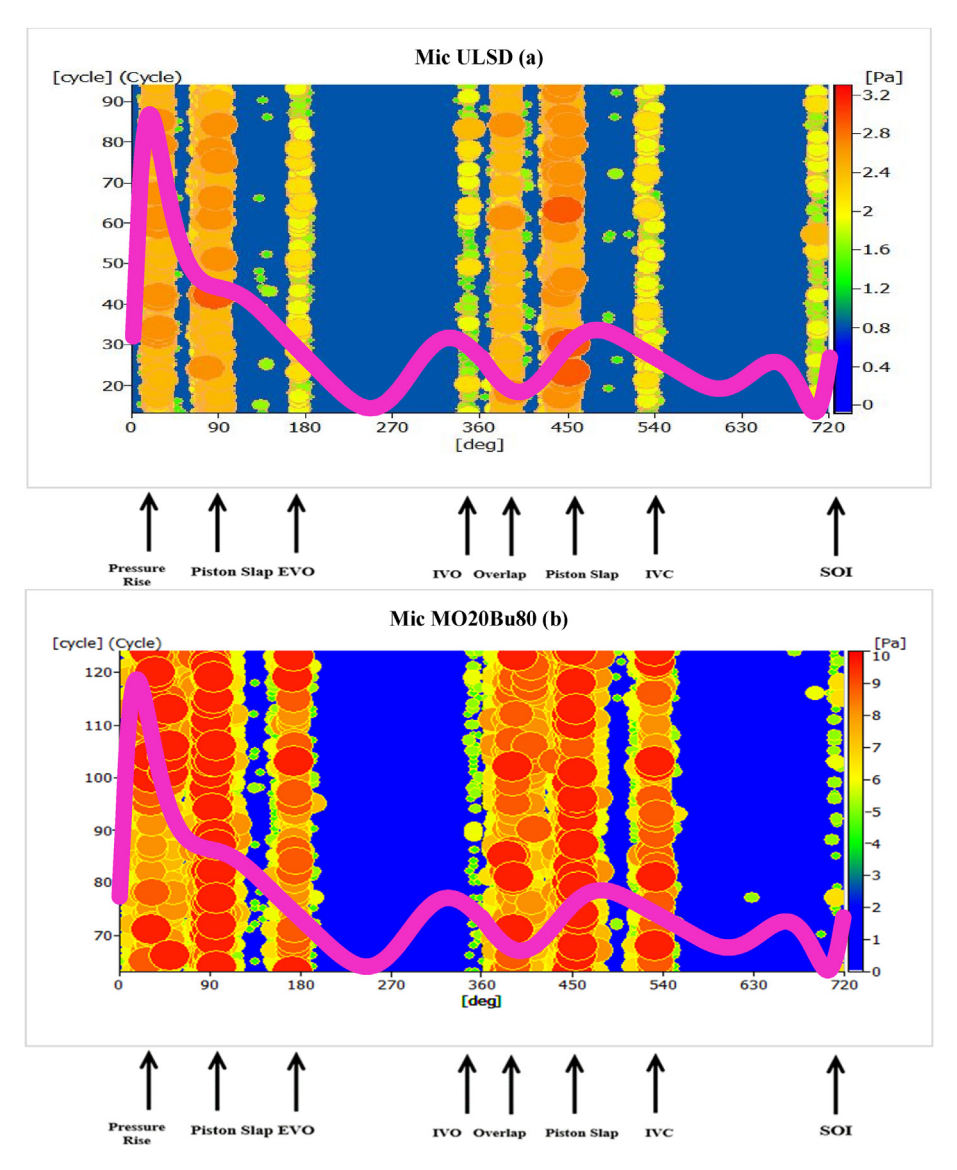


Fig. 18. Mic cylinder ULSD (a) & MO20Bu80 (b).

In the Fig. 19, (a) & (b), the semi-sinusoidal curves represent the valves' motion during the cycle, with overlap at the 360-375 CAD. The vertical bands in the graphs represent the vibrations recorded at valves' overlap and at the injection event before the 720 CAD line. The MO20Bu80 shows lowest vibrations in the Z-axis (cylinder direction, (b) graph) compared with the ULSD ((a) graph) since the intake valve port is wet from n-Butanol PFI.

5.4. Point source measurements

The graphs in the following Fig. 20, confirm the Sound Campbell plots results. In the top (a) figure, the louder sound for the MO20Bu80 as much as 10 dB (A) in the cylinder direction was recorded compared with ULSD in CDC. This could be explained by higher AHRR of the MO20Bu80 [51]. In the bottom figure (b), the FFT confirms the CPB graph because at the lower frequencies of the FFT the mechanical parts in the engine correlate in half orders. The first peak is the main harmonic (engine speed) in terms of

frequency (25 Hz), and the next peak occurs at half the frequency distance of the primary frequency. The point source sound tests from Fig. 20 show the key differences in the mechanical noise and the overall noise in the cylinder direction of the engine. Overall, the Methyl Oleate with n-Butanol in RCCI follow the trend of having a louder combustion event than that of ULSD in CDC. This could be explained the physical and chemical properties of the combination of fuels and RCCI combustion characteristics.

5.5. Real-time noise source identification

Combustion noise is the most notable with differences found in the sound array analysis [14–16]. In the array analysis for combustion only, the RCCI fuel was 6 dB (A) higher than classical diesel combustion (ULSD) overall. Using frequencies that closely correlate with sound produced by the engine during combustion, simplifies the analysis for the acoustic array as can be observed from Figs. 22–24. Figs. 22–24 focused on the 250–2.5k Hz range that

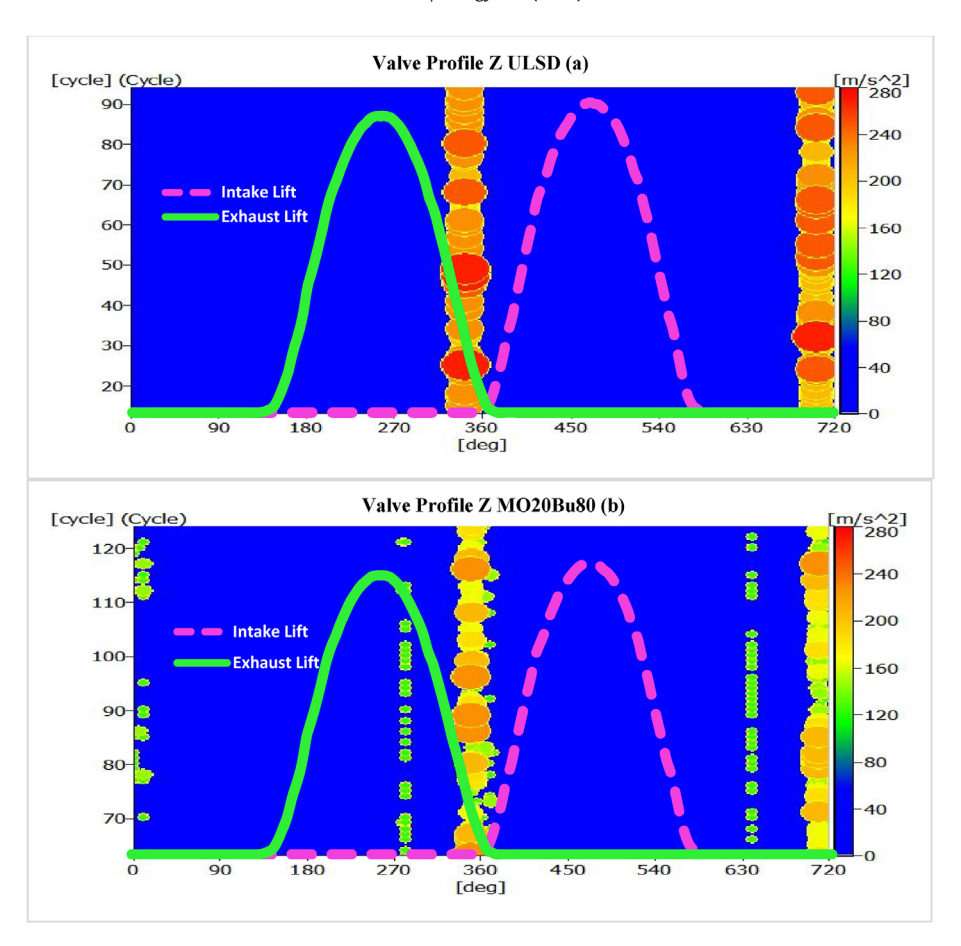


Fig. 19. Z-axis (cylinder) ULSD (a) & MO20Bu80 (b).

was observed in previous literature [16] by Chen at al to be the appropriate combustion range. The yellow colors represent the highest level of sound and green representing the lowest level of sound and their location. As can be seen in Figs. 22 and 23, MO20Bu80 has the higher range of sound for the sample frequency

chosen. In Fig. 25, the results of the array analysis can be seen. The fuel that has the most sound produced is the MO20Bu80. The array analysis, at each frequency chosen, averages the sound produced at that frequency. Therefore, across the frequency range chosen MO20Bu80 has a decibel reading of as much as 5 dB above ULSD in

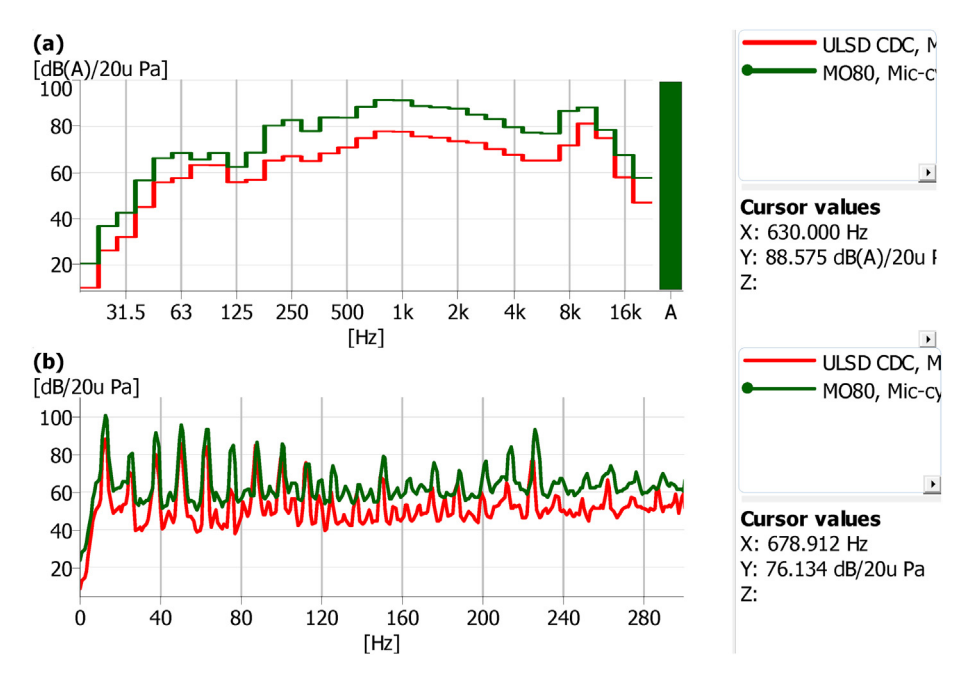


Fig. 20. Mic confirmation of data CPB (a) and FFT (b).

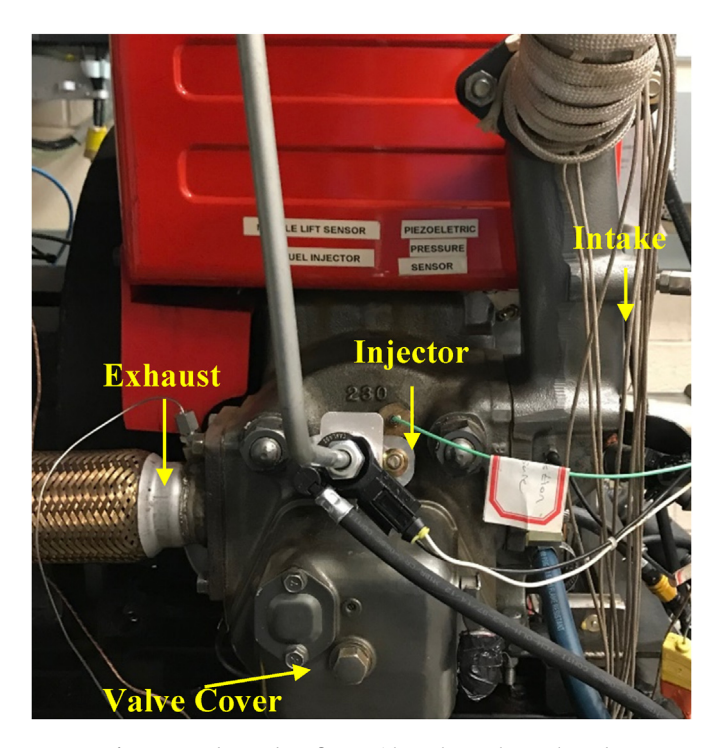


Fig. 21. Sound Array base figure without the results overlapped.

the central points of the combustion range (400 Hz - 1 kHz). The image of the engine used in the Acoustic array camera is shown in Fig. 21 without the db level overlay, for additional clarity.

The acoustic array analysis (facing the cylinder) displayed noise differences above the 3 dB (A) threshold at the combustion ranges established in literature [2]. This concludes that the planar form of the acoustic array did show that RCCI has its own acoustic spectrum compared to CDC, and this is because of the wider range and higher sound levels produced by RCCI. The averaging method allows the measurement of specific frequencies and pinpointing the sources of those frequencies. However, the frequency-by-frequency band analysis shows that Methyl Oleate is louder in combustion compared to the ULSD in CDC.

5.6. The accelerometer based CPB and fast fourier vibration analysis

For the vibration analysis, using an $\frac{1}{3}$ octave bandwidth method is for the purpose of visibility and better understanding, but the CPB analysis has basis on the FFT results produced from the accelerometer [52-55]. The bottom axis on each graph (Figs. 26 and 27) is the frequency at which the vibrations occur, and the left axis displays the acceleration in logarithmic scale in the top graph. The top graph has the frequency ranged only to 240 Hz to show the mechanical differences in vibrations; in this case, the y-axis of this graph is in a linear format for easy reading. It is confirmed that RCCI strategy produces higher accelerations than ULSD in the Z-cylinder direction as seen in Figs. 26 and 27; the change by the (overall) RCCI strategy are as much as 2.5 times (on average) the vibrations produced by the ULSD. This has prevalence in the range from 250 Hz to 2 kHz. The amount in terms of absolute values, they are between 5 (m/s^2) and 10 (m/s^2) overall difference. In the vibrations graph for mechanical vibrations (Fig. 26), the highest vibration at the 1500rpm (25 Hz) point is the ULSD CDC.

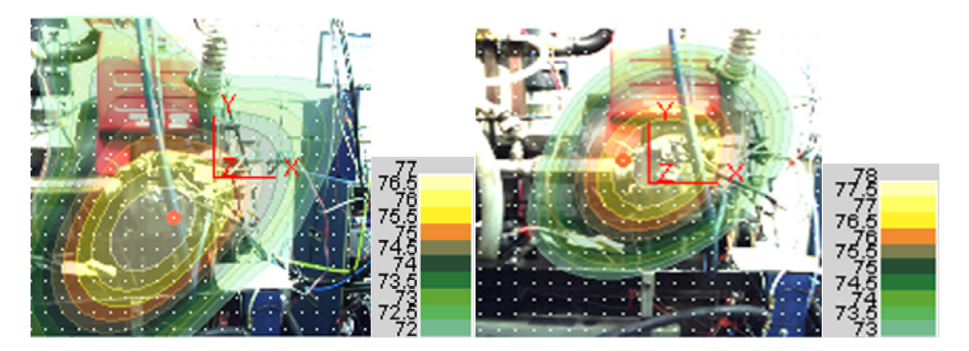


Fig. 22. 2.5k Hz cylinder acoustic array contours ULSD (left), MO20Bu80 (right).

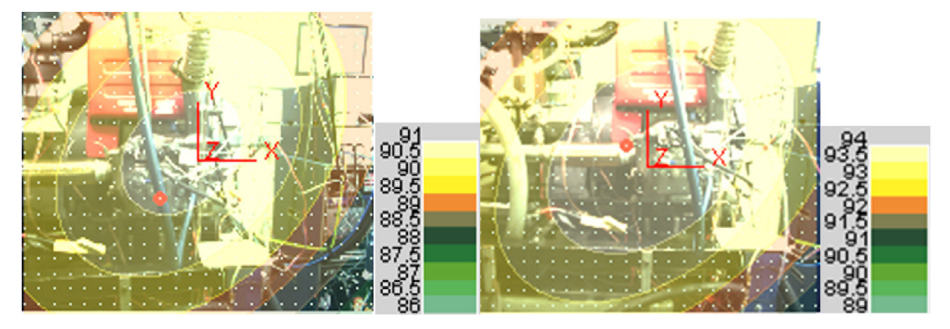


Fig. 23. 800 Hz cylinder ULSD in CDC (left) and MO80 (right).

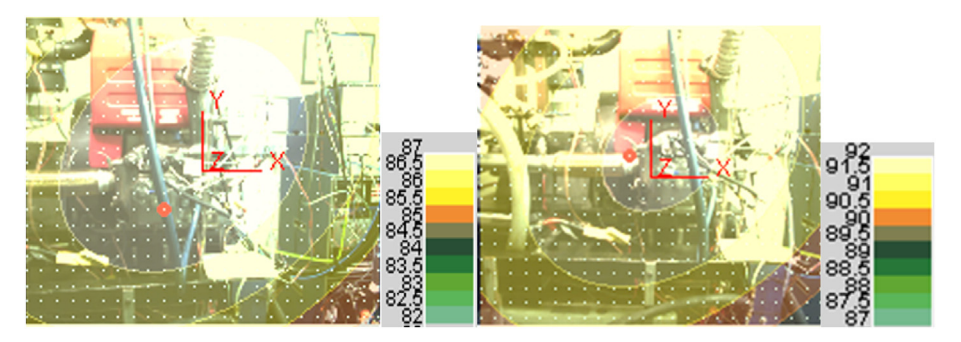


Fig. 24. 630 Hz cylinder ULSD in CDC (left) and MO80 (right).

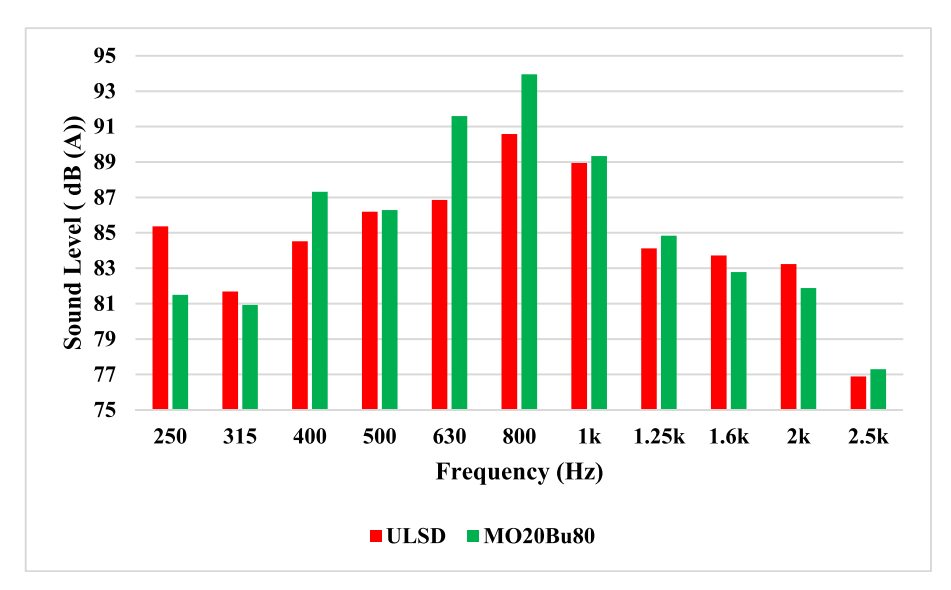


Fig. 25. Sound Level vs Frequency (Acoustic Array).

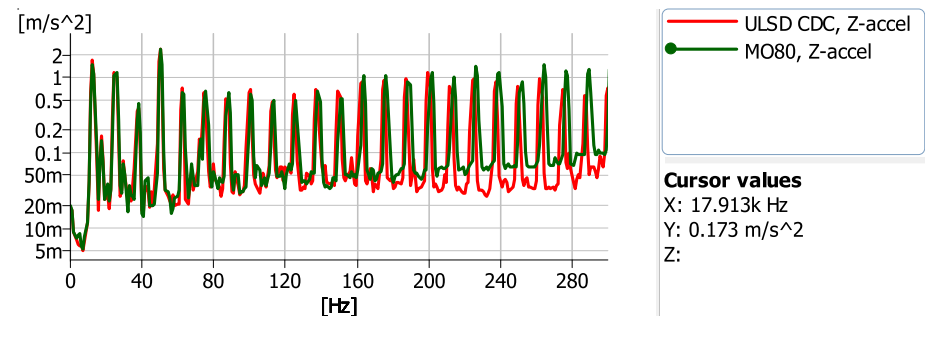


Fig. 26. Mechanical vibrations (FFT).

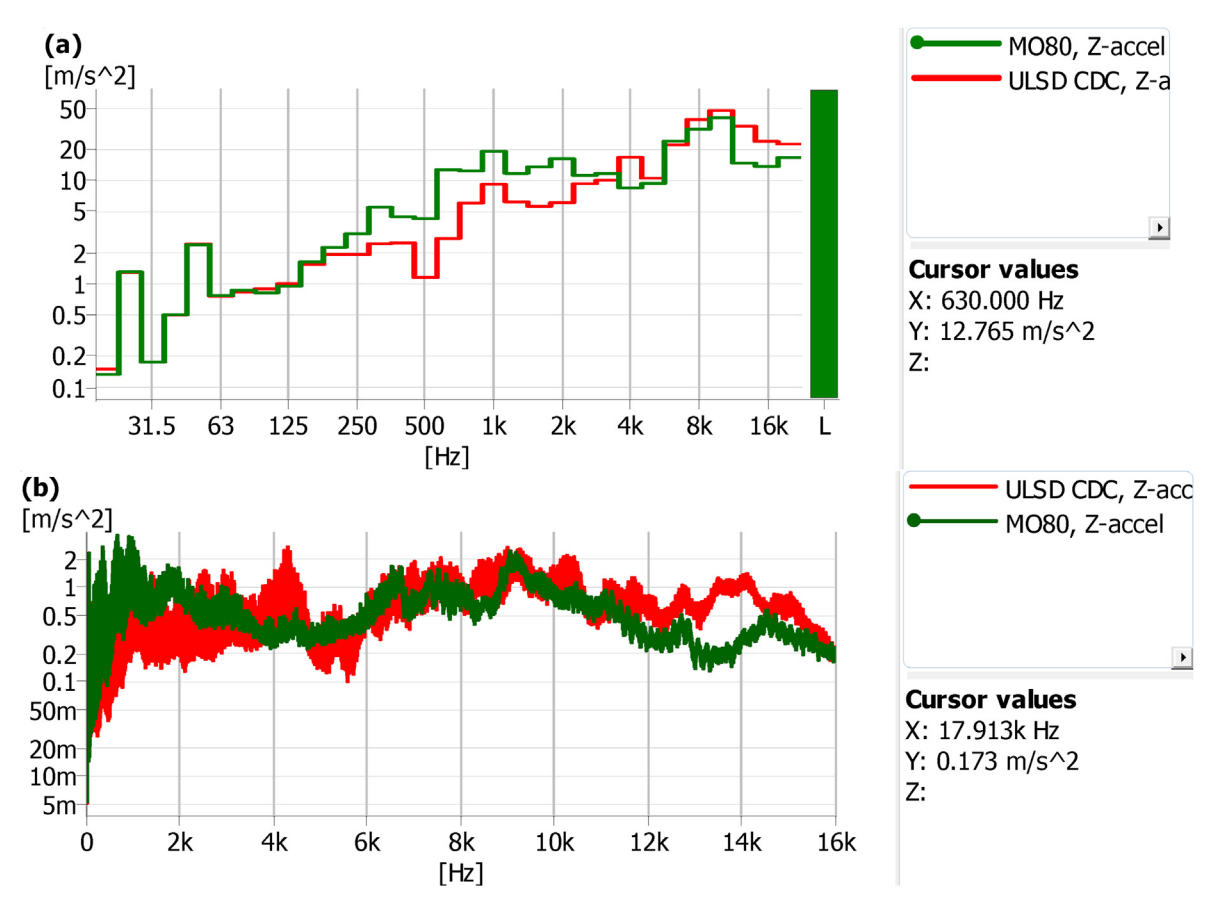


Fig. 27. Vibrations overall in CPB (a) and FFT (b).

6. Conclusion

A comprehensive study with n-Butanol and Methyl Oleate in Combustion, Noise and Vibrations was completed for RCCI in comparison to ULSD CDC at 1500 RPM under a load of 6 bar IMEP.

The in-cylinder pressure results show that the RCCI strategy has an increased pressure gradient than ULSD. This happens due to the increased ignition delay by the n-butanol that absorbs a high amount of heat to vaporize and it has also a very low cetane number. As a result, in the case of the MO20Bu80, the maximum apparent heat release rate is much higher due to accumulation of fuel in the combustion chamber because of the longer ignition delay due to cooling effect of n-butanol - phenomenon reflected in the lower compression pressure BTDC. The diffusion stage of combustion found in the CDC case, is disappeared in the RCCI strategy. In concurrence with the diffusion stage of combustion, while noticeable with ULSD, the diffusion burn of MO20Bu80 fades showing only a large premixed phase.

For the crank-angle-domain analysis the pressure, rotary encoder, and microphones were applied to acquire the data. The significant points of study during the cycle for sound were found to be at 10 CAD after 0 (TDC) the combustion noise, and the next band the piston slap occurring at the 90 CAD ATDC mark. Before 180 CAD it is the sound from EVO, and the 360 CAD is the IVO and start of valve overlap. At 450 CAD next perceptible piston slap occurs, and at 540 CAD the intake valve closes. At 10° before 720 CAD the injection event occurs. In the cylinder direction (Z-axis), MO20Bu80 in combustion has the highest sound pressure measurements at 10 Pa. USLD in combustion achieved a reduced sound level at 3.2 Pa.

For crank-angle-domain with vibrations the MO20Bu80 displays the lowest vibrations in the cylinder direction compared with the ULSD.

For the overall point source measurements, the loudest sound is produced by MO20Bu80 combustion, with values as much as high 10 dB (A) in the cylinder direction compared with ULSD in CDC. This could be explained by higher AHRR and combustion pressure gradient of the MO20Bu80. Using the CPB analysis confirms the decibel noise levels produced by changing the fuel in combustion.

Array analysis used a form of CPB analysis to bring more detail in to the data by looking at each frequency within the combustion range of 250 Hz to 2.5 kHz. In the array analysis, for combustion only, the RCCI fuel produced a 6 dB (A) increase above ULSD overall. Across the frequency range selected MO20Bu80 has a decibel reading of 5 dB above ULSD in the central points of the combustion range (400 Hz - 1 kHz). The acoustic array analysis exhibited noise differences above the 3 dB (A) threshold at the combustion ranges. This concludes that the planar method of the acoustic array did display that RCCI has its particular acoustic spectrum compared to CDC, and this is because of the wider range and higher sound levels created by RCCI. The frequency-by-frequency band analysis displays that Methyl Oleate is louder in combustion compared to the ULSD in CDC.

The vibrations showed the differences primarily in the combustion range, just like the Acoustic Array band analysis. This study found that RCCI strategy produces higher accelerations than ULSD in the Z-cylinder direction. During the piston tilt, the top of the piston skirt and the bottom of the opposing edge of the skirt slap the cylinder and produce vibrations. The overall vibrations levels

for the RCCI injection and combustion strategy are much higher than those of the ULSD in CDC. The difference produced by the RCCI strategy are on average 2.5 times higher than the vibrations produced by the ULSD. This has prevalence in the range from 250 Hz to 2 kHz. The quantity in terms of absolute values, are between 5 (m/ $\rm s^2$) and 10 (m/s²) overall difference. In the vibrations graph for mechanical vibrations, the peak vibration at the 1500-rpm (25 Hz) point is the ULSD CDC.

This study showed that Methyl Oleate can be used as an alternative fuel for full body biodiesel in RCCI combustion, however with the cost of a louder combustion than that of ULSD in CDC at the tested conditions.

CRediT authorship contribution statement

Valentin Soloiu: Supervision, Project administration, Funding acquisition, Conceptualization, Formal analysis, Writing - review & editing. Aliyah R. Knowles: Conceptualization, Investigation, Data curation, Formal analysis. Cesar E. Carapia: Formal analysis, Visualization, Writing - original draft. Jose D. Moncada: Formal analysis, Visualization, Writing - original draft, Data curation, Writing review & editing. Justin T. Wiley: Formal analysis, Visualization, Writing - original draft, Data curation, Validation. Margaret Kilpatrick: Data curation. Johnnie Williams: Data curation, Visualization. Mosfequr Rahman: Formal analysis. Marcel Ilie: Writing - original draft, Writing - review & editing.

Acknowledgements

Acknowledgment of Sam Olesky from Kistler, Charles McGuffy and Janusz Waszkielewicz from PAC, Matt Viele from Vieletech, Daniel Stockton from AVL, Tanner Smith, Tony Frazer, Ryan Salmon, and Alfonso Moreira from B&K, Joseph Wolfgang von Malvern and Richard Frazee from Singularity Scientific for their technical support. This paper is based upon work supported by the National Science Foundation, United States, under Grant No. 1609524.

Appendix A. Supplementary data

Supplementary data to this article can be found online at https://doi.org/10.1016/j.energy.2020.118183.

References

- o NA. Engineering, technology for a quieter America. Washington, DC: The National Academies Press; 2010. https://doi.org/10.17226/12928.
- [2] Labor US Do. Occupational safety and Health administration. United States Department of Labor; 2018 [Online]. Available: https://www.osha.gov/SLTC/ noisehearingconservation/index.html. [Accessed 18 January 2019].
- [3] Bhansali SS, Kongre DU, Shirgire N, Bodade P. Analysis and study of vibrations in view of combustion gas forces for diesel engine. IOSR J Mech Civ Eng 2013;vol. 6(no. 3):48–55.
- [4] Carder D, Ryskamp R, Besch M, Thiruvengadam. Emissions control challenges for compression ignition engines. Procedia IUTAM 2017;vol. 20:103–11. https://doi.org/10.1016/j.piutam.2017.03.015.
- [5] Soloiu V, Simons E, Muinos M, Harp S. NVH of RCCI withDI ULSD and PFI with 50% n-Butanol. In: Internal combustion engine division fall technical conference; 2015. https://doi.org/10.1115/ICEF2015-1161. Houston, TX.
- [6] Simons E, Soloiu V. Reduction of aircraft gas turbine noise with new synthetic fuels and sound insulation materials," transportation research record. Journal of the Transportation Research Board 2017;2603:50–64. https://doi.org/ 10.3141/2F2603-06
- [7] Soloiu V, Simons E, Munios M, Harp S, Knowles A, Molina G. Sound and vibration levels of CI engine with synthetic kerosene and n-butanol in RCCI. In: SAE world congress and exhibition 2016; 2016. https://doi.org/10.4271/2016-01-1306. Detroit, MI.
- [8] Arnon L, Boni M, Chiavola O, Conforto S, R.E.. Diesel engine combustion monitoring through block vibration signal analysis. In: SAE international; 2009. https://doi.org/10.4271/2009-01-0765. Detroit, MI.
- [9] Kim YS, Lee DJ. Numerical analysis of internal combustion engine intake noise with a moving pistion and a valve. J Sound Vib 2001;vol. 241(no. 5):895–912.

- https://doi.org/10.1006/jsvi.2000.3339.
- [10] Badawi BA, Shahin MA, Kolosy M, Shedied SA, Elmaihy A. Identification of diesel engine cycle events using measured surface vibration. Detroit, MI: SAE International World Congress; 2006, https://doi.org/10.4271/2006-32-0097.
- [11] Miura Y, Kojima N. Noise generating mechanism at idling for a four-cylinder in- line diesel engine. In: SAE 2003 noise & vibration conference and exhibition. United States: Warrendale; 2003. https://doi.org/10.4271/2003-01-1720. doi.org/.
- [12] Goldwine G, deBotton G, Rivin B, Sher E. Studying the relationship between the vibration signature and the combustion process in diesel engines. In: SAE world congress & exhibition; 2004. https://doi.org/10.4271/2004-01-1786. Detroit. MI.
- [13] Wissink M, Wang Z, Splitter D, Shahlari A, Reitz R. Investigation of pressure oscillation modes and audible noise in RCCI, HCCI, CDC. In: SAE 2013 world congress & exhibition, detroit, MI; 2013. https://doi.org/10.4271/2013-01-1652.
- [14] Liu S, Gu F, Ball A. Detection of engine valve faults by vibration signals measured on the cylinder head. Proc Inst Mech Eng Part D J Automob Eng 2006;220(3):379–86. https://doi.org/10.1243/09544070[AUTO90.
- [15] Suh I. Combustion on radiation noise and mount vibration from a V8 gasoline engine. In: Noise & vibration conference and exhibition. Michigan: Traverse City; 2003. https://doi.org/10.4271/2003-01-1730.
- [16] Chen GS. Vehicle noise, vibration, and sound quality. Warrendale, PA: SAE International; 2012, ISBN 978-0-7680-3484-4.
- [17] Adams ML. Rotating machinery vibration: from analysis to troubleshooting. New York, NY: Marcel Dekker; 2001.
- [18] Soloiu VA, Jenzer J. Active torsional vibration control for large two stroke marine diesel engines. In: SAE international congress and exhibition; 1998. https://doi.org/10.4271/981041. Detroit, MI.
- [19] Kimura J, Kobayashi S, Hoshina K, Kawase K, M.K., Yammamoto A. Crankshaft impact noise and three-dimensional vibration. In: SAE 2014 international powertrain. Birmingham, United Kingdom: Fuels & Lubricants Meeting; 2014. 10.4271/2014- 01-2863.
- [20] Dolatabadi N, Theodossiades S, Rothberg SJ. On the identification of piston slap events in internal combustion engines using tribodynamic analysis. Mech Syst Signal Process 2014;vol. 58(no. 59):308–24. https://doi.org/10.1016/ j.ymssp.2014.11.012.
- [21] Shahabuddin M, Liaquat AM, Masjuki HH, Kalam MA, Mofijur M. Ignition delay, combustion and emission characteristics of diesel engine fueled with biodiesel. Renew Sustain Energy Rev 2013;21:623–32. https://doi.org/ 10.1016/j.rser.2013.01.019.
- [22] Howarth VCH, Griffin MJ. The annoyance caused by simultaneous noise and vibration from railways. J Acoust Soc Am 1991;vol. 89(no. 5):2317–23. https://doi.org/10.1121/1.400922.
- [23] B., Kjaer. Bruel & kjaer. " [Online]. Available: [Accessed 2017 November 2017], https://www.bksv.com/media/doc/bn1251.pdf.
- [24] B., Kjaer. Noise source identification techniques:simple to advanced applications, [Online]. Available: https://www.bksv.com/doc/bn1251.pdf. [Accessed 17 March 2018].
- [25] Kjaer Bruel. Bruel & kjaer. "23 March 2003. [Online]. Available: https://www.bksv.com/-/media/literature/Technical-Review/bv0056.ashx. [Accessed 6 July 2018].
- [26] Chiariotti P, Battista G, Ettorre M, Castellini. Average acoustic beamforming in car cabins: an automatic system for acoustic mapping over 3D surfaces. Appl Acoust 2018;129:47–63. https://doi.org/10.1016/j.apacoust.2017.07.009.
- [27] Van Veen BD, Buckley KM. Beamforming: a versatile approach. IEEE ASSP Mag April 1988:4–24.
- [28] Haynes T. Spectral signal. March 2006. [Online]. Available: https://web.archive.org/web/20060316172123/http://www.spectrumsignal.com/publicatio ns/beamform_primer.pdf. [Accessed 12 June 2018]. 16.
- [29] Gaubert R, Soloiu V, Moncada J, Wiley T, Williams J, Harp S, Ilie M, Molina G. Reactivity controlled compression ignition and low. Renewable Energy; 2018. p. 1–17. https://doi.org/10.1016/j.renene.2018.09.047.
- [30] Soloiu V, Moncada J, Gaubert R, Knowles A, Molina G, Illie M, Harp S, Wiley J. Reactivity Controlled Compression Ignition combustion and emissions using n-butanol and methyl oleate. Energy 2018;165:911–24. https://doi.org/ 10.1016/j.energy.2018.09.181.
- [31] American Society for Testing, Materials International. Standard test method for determination of derived cetane number (DCN) of diesel fuel oils—ignition delay and combustion delay using a constant volume combustion chamber method. West Conshohocken, PA, United States: ASTM International; 2014. p. 1–14.
- [32] Knothe G, Matheaus AC, Ryan TWI. Cetane numbers of branched and straightchain fatty esters determined in an ignition quality tester. Fuel 2002;82: 971–5. https://doi.org/10.1016/S0016-2361(02)00382-4.
- [33] Han D, Duan Y, Wang C, Lin H, Huang Z. Experimental study on injection characteristcs of fatty acid esters on a diesel engine common rail system. Fuel 2014;123:19–25. https://doi.org/10.1016/j.fuel.2014.01.048.
- [34] J.E., Liu T, Yang WM, Li J, Gong J, Deng Y. Effects of fatty acid methyl esters proportion on combustion and emission charceristics of a biodiesel fueled diesel engine. Energy Convers Manag 2016;117:410–9. https://doi.org/10.1016/j.enconman.2016.03.021.
- [35] National Center for Biotechnology Information. PubChem compund database. National Institute of Health; 09 June 2018 [Online]. Available: https://pubchem.ncbi.nlm.nih.gov/compound/5364509. [Accessed 12 June 2018].

- [36] Valentin S, Muinos M, Harp S, Naes T, Gaubert R. Combustion and emissions characteristics of dual fuel premixed charge compression ignition with direct injection of synthetic FT kerosene produced from natural gas and port fuel injection of n- butanol. In: SAE international world congress 2016,; 2016. https://doi.org/10.4271/2016-01-0787. Detroit, MI.
- [37] Muinos M, Soloiu V, Moncada J, Gaubert R, Gustavo M, Williams J. Experimental investigation on the combustion and emissions characteristics of n-butanol/GTL and n- butanol/diesel blends in a single-cylinder MD-CI engine. SAE international world congress 2017. 2017. https://doi.org/10.4271/2017-01-0719. Detroit, MI.
- [38] Heywood JB. Internal combustion engine fundamentals. New York, USA: Tata McGraw-Hill; 2011.
- [39] Gaubert R, Soloiu V, Moncada J, Wiley T, Williams J, Harp S, Ilie M, Molina G. Reactivity controlled compression ignition and low temperature combustion of Fischer- Tropsch Fuel Blended with n-butano. Renew Energy 2018;134: 1173–89. https://doi.org/10.1016/j.renene.2018.09.047.
- [40] Soloiu V, Gaubert R, Muinos M, Moncada J, Beyerl T, Molina G, Williams J. Performance of an indirect injected engine operated with ULSD#2 blended with fischer- tropsch synthetic kerosene. In: SAE international world congress 2017; 2017. https://doi.org/10.4271/2017-01-1283. Detroit, MI.
- [41] Liu H, Ma G, Ma N, Zheng Z, Huang H, Yao M. Effects of charge concentration and reactivity stratification on combustion and emission characteristics of a PFI-DI dual injection engine under low load condition. Fuel 2018;231:26–36. https://doi.org/10.1016/j.fuel.2018.05.027.
- [42] Zheng Z, Xia M, Liu H, Wang X, Yao M. Experimental study on combustion and emissions of dual fuel RCCI mode fueled with biodiesel/n-butanol, biodiesel/ 2,5- dimethylfuran and biodiesel/ethanol. Energy Feb. 2018;148:824–38. https://doi.org/10.1016/j.energy.2018.02.015.
- [43] Soloiu V, Weaver J, Ochieng H, Duggan M, Davoud S, Vlcek B, Jenkins C, Butts C. Experimental study of combustion and emissions characteristics of methyl oleate, as a surrogate for biodiesel, in a direct injection diesel engine. SAE technical paper series. Aug. 2013. https://doi.org/10.4271/2013-01-1142.
- [44] Soloiu V, Lewis J, Covington A, Nelson D, Schmidt N. Oleic methyl ester investigations in an indirect injection diesel engine; stage one: combustion investigations. SAE International Journal of Fuels and Lubricants Dec.

- 2011;4(1):58-75. https://doi.org/10.4271/2011-01-0616.
- [45] Allen C, Toulson E, Tepe D, Schock H, Miller D, Lee T. Characterization of the effect of fatty ester composition on the ignition behavior of biodiesel fuel sprays. Fuel 2013;111:659–69.
- [46] Liu H, Tang Q, Ran X, Fang X, Yao M. Optical diagnostics on the reactivity controlled compression ignition (RCCI) with micro direct-injection strategy. Proc Combust Inst 2018;37(4):4767-75. https://doi.org/10.1016/ j.proci.2018.06.180.
- [47] Han D, Duan Y, Chunhai W, Lin H, Huang Z. Experimental study on injection characteristics of fatty acid esters on a diesel engine common rail system. Fuel 2014;123:19–25.
- [48] Han D, Duan Y, Wang C, Lin H, Huang Z, Margaret WS. Experimental study of the two- stage injection process of fatty acid esters on a common rail injection system. Fuel 2016:163:214–22.
- [49] van Basshuysen R, Schafer F. Internal combustion handbook: basics, components, systems, and perspectives. Warrendale, PA: SAE International; 2004.
- [50] Nag S, Sharma P, Gupta A, Dhar A. Combustion, vibration and noise analysis of hydrogen- diesel dual fuelled engine. Fuel 2019;241:488–94. https://doi.org/ 10.1016/j.fuel.2018.12.055
- [51] Khaira SS, Singh A, Jansons M. Effect of injection parameters and strategy on the noise from a single cylinder direct injection diesel engine. In: ASME 2011 internal combustion engine division fall technical conference. West Virginia: Morgantown; 2011. 10.1115/ICEF2011- 60148.
- [52] Vavra J, Bohac SV, Manofsky L, Lavoie G, Assanis D. Knock in various combustion modes in A gasoline-fueled automotive engine. In: ASME 2011 internal combustion engine division fall technical conference. WV: Morgantown; 2011. https://doi.org/10.1115/ICEF2011-60124.
- [53] Mashkournia M, Audet A, Koch CR. Knock detection and control in an HCCI engine using DWT. In: ASME 2011 internal combustion division fall technical conference. WV: Morgantown; 2011. https://doi.org/10.1115/ICEF2011-60076
- [54] Broch JT. The application of the Bruel & kjaer measuring systems. Denmark, Norway: Bruel & Kjaer; 1980.
- [55] Randall RB, Tech B. Frequency analysis. Denmark: Bruel & Kjaer; 1987.